ELECTROANALYSIS
An International Journal Devoted to Electroanalysis, Sensors and Bioelectronic Devices

Nanoporous Pt(Au) alloys for the enhanced, non-enzymatic detection of hydrogen peroxide under biofouling conditions

Journal:	*Electroanalysis*
Manuscript ID	elan.202100568.R1
Wiley - Manuscript type:	Research Article
Date Submitted by the Author:	01-Nov-2021
Complete List of Authors:	Khan, Md. Rezaul; Virginia Commonwealth University, Chemistry Silva, Tiago; Universidade Federal de Viçosa, Department of Chemistry Fatibello-Filho, Orlando; Universidade Federal de São Carlos, of Chemistry Collinson, M.; Virginia Commonwealth University, Chemistry; USA Farghaly, Ahmed; Argonne National Laboratory, Chemical Sciences and Engineering Division
Keywords:	sensor, anti-biofouling, chemical dealloying, high surface area electrodes, nanoporous platinum

Nanoporous Pt(Au) alloys for the enhanced, non-enzymatic detection of hydrogen peroxide under biofouling conditions

Rezaul K. Khan,[†,a] Tiago A. Silva,[‡, ‖,a] Orlando Fatibello-Filho[‡], Maryanne M. Collinson[†]* and Ahmed A. Farghaly[□]

[†]Department of Chemistry, Virginia Commonwealth University, Richmond, Virginia 23284-2006, United States
*E-mail: mmcollinson@vcu.edu
ORCID ID orcid.org/0000-0001-6839-5334

[□]Chemical Sciences and Engineering Division, Argonne National Laboratory, Lemont, Illinois 60439-4801, United States
[□]Chemistry Department, Faculty of Science, Assiut University, Assiut 71516, Egypt

ORCID ID orcid.org/0000-0001

[‡]Department of Chemistry, Federal University of São Carlos, São Carlos, CEP: 13560-970, SP, Brazil
ORCID ID orcid.org/0000-0002-6923-2227

[‖]Department of Chemistry, Federal University of Viçosa, Viçosa, CEP: 36570-900, MG, Brazil
ORCID ID orcid.org/0000-0002-7202-789X

[a]These authors contributed equally to this work and both should be considered as first author

Graphical Abstract

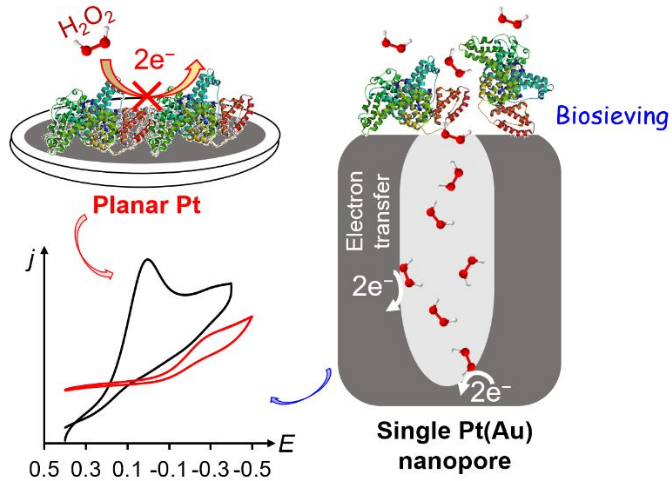

Abstract

The non-enzymatic electrochemical sensing of hydrogen peroxide (H_2O_2) is described. This study utilized a 3D bicontinuous nanoporous platinum-gold alloy-based sensor (NP-Pt(Au) electrode), which has a morphology that resembles a molecular sieve. SEM and CV were used to evaluate the morphological and electrochemical characteristics of the NP-Pt(Au) electrodes. The cathodic voltammetric response of H_2O_2 was enhanced at the NP-Pt(Au) as compared to planar Pt electrodes. The nanoporous electrode was able to maintain the H_2O_2 voltammetric profile even in the presence of the biofouling agent, serum albumin. Its application as a non-enzymatic sensor for the amperometric measurement of H_2O_2 was explored.

Keywords: high surface area electrodes, nanoporous platinum, chemical dealloying, anti-biofouling, sensor

1. Introduction

Hydrogen peroxide (H_2O_2) is a molecule of great importance. It is an unusual molecule in the sense that it can serve as an oxidizing or reducing agent depending on the conditions.[1-2] The public knows it as a well-known disinfectant and an additive in toothpaste. H_2O_2 has also been widely used in chemical and food industries;[1-2] it plays a pivotal role in redox signaling and oxidative stress[3-4] and has been used as an oxidant in fuel cells serving as a possible replacement for oxygen.[5] H_2O_2 also serves as an important molecule for the detection of many biomolecules such as glucose because it's the byproduct of the glucose oxidase catalyzed reaction.[1-2] Due to its importance, the sensitive, accurate, and precise detection and measurement of H_2O_2 in simple and complex environments are essential and highly significant.[1-2]

Different methods have been reported for the detection and measurement of hydrogen peroxide including electrochemistry, fluorometry, titrimetry, spectrophotometry, and chemiluminescence.[6-7] Electrochemical methods stand out among the numerous analytical techniques because of their low cost, simplicity, high sensitivity, and wide linear detection range.[1, 7] There are numerous enzymatic electrochemical sensors for selective and sensitive analysis of H_2O_2 that are based on the immobilization of enzymes such as hemoglobin, horseradish peroxidase, and myoglobin.[1] However, the stability, cost, and usefulness for measurements undertaken in conventional environments can be limitations of such sensors.[8-9] In this regard, a non-enzymatic sensor with direct electron transfer between analyte and electrode surface is an appealing alternative.[9-11] Many different electrode materials have been used for the detection of hydrogen peroxide including nanoporous metals and materials,[1, 4, 12-17] metallic nanoparticles,[18] and carbon-based materials.[10, 19] Among the numerous types of nanoporous metals, nanoporous platinum is particularly useful for the determination of H_2O_2 because of its improved electron transfer kinetics.[20-21]

Though the detection and measurement of analytes on non-enzymatic sensors are attractive, in a complex medium such as blood, the electrode surface can be seriously poisoned due to the presence of numerous proteins that adsorb and occupy the catalytic sites on the flat metal surface of the sensor.[22-24] The electrochemical signals are strongly affected by this adsorption and continued operation.[25-26] Nanoporous metals with an engineered 3D bicontinuous framework are able to minimize the degree of biofouling of the electrode surface.[27-29] These nanoporous metals have a unique sieving-like mechanism where larger proteins responsible for poisoning the sensor surface are prevented from reaching the inner pristine metal surface while small redox molecules are not.[27-29] Recently, Farghaly et al. have synthesized a unique 3D bicontinuous nanoporous platinum-gold alloy sensor having a pore morphology that resembles a molecular sieve.[30] In this work, we report on the non-enzymatic detection and measurement of H_2O_2 using these unique nanoporous platinum-gold bimetallic alloys in the presence and absence of the biofouling protein, bovine serum albumin. We show that these electrodes can quantitatively detect H_2O_2 in complex biofouling environments.

2. Experimental section

2.1. Materials and solutions

All chemical reagents were of analytical degree and used as received from the respective suppliers (Fisher Scientific or Sigma-Aldrich). Bovine serum albumin (BSA) was purchased as a lyophilized powder. Aqueous solutions were prepared using ultrapure water obtained from a Millipore Milli-Q® water purification system. The commercial plating solutions (Elevate Platinum 7810 RTU and Silver 1025 RTU) were purchased from Technic

Inc. Fetal bovine serum (FBS) (Quality Biological Inc.) was kindly provided by Dr. Farrell (Department of Chemistry, VCU). A 0.1 M H_2O_2 stock solution was daily prepared in 0.1 M phosphate buffer/ 0.1 M KCl, pH 7.4 supporting electrolyte solution.

2.2. Instrumentation

Scanning electron microscopy (SEM) was performed on Hitachi SU 70 field emission scanning electron microscope. Electrochemical assays were carried out on a CHI 660E electrochemical workstation (CH Instruments, Inc.). A 10-mL three-electrode electrochemical cell was adopted. A commercial planar Pt or NP-Pt(Au) were used as the working electrode while a Pt wire and a Ag/AgCl (0.1 M KCl) were used as the counter and reference electrodes, respectively. The geometric area (0.079 cm^2) of NP-Pt(Au) electrode was defined by a 1/8-inch circle hand punched into a piece of tape, which was carefully placed on the electrode surface.

2.3. Preparation of NP-Pt(Au) electrode

Gold-coated test slides (EMF, Dynasil) were cut into appropriate sizes and sonicated in ethanol, DI water followed by drying with nitrogen flow, and plasma cleaned. The cleaned Au slide was used as a substrate to deposit the Pt-Ag alloy electrochemically. To deposit the alloy, the gold electrode was placed in a solution containing 9 mL of Pt-elevate solution, 20 mg platinum salt, K_2PtCl_4, and 100 µL of the AgCN plating solution (CAUTION: cyanide salts are highly toxic and appropriate precautions must be taken when using them). A controlled potential (−1.0 V) was applied for 10 minutes to electrodeposit the Pt-Ag alloy film. After washing several times with DI water, the gold substrate with the electrodeposited Pt-Ag alloy was placed in an oven at 65 ^{0}C for 30 min followed by drying and annealing in a muffle furnace.[30] The annealed sample was dealloyed by submerging in 1:1 (v:v) DI water:nitric acid (CAUTION: HNO_3 is a highly corrosive and dangerous acid and must be handled with extreme caution using protective equipment such as gloves, safety goggles, and protective clothing under a fume hood) to remove Ag.[30] The dealloyed porous electrode was washed four times in DI water, each time for 10 minutes, followed by drying with nitrogen gas. The resulting NP-Pt(Au) electrode is ready to use for H_2O_2 non-enzymatic determination.

2.4. Electrochemical assays

Cyclic voltammetry (CV) was applied to study the responsivity of the target analyte, H_2O_2, using the commercial planar Pt and in-house constructed NP-Pt(Au) electrodes in the test solutions. The analytical determination of H_2O_2 was achieved by chronoamperometry at a fixed potential of −0.1 V *vs*. Ag/AgCl (0.1 M KCl). For the construction of the analytical curve, the chronoamperometric curves were registered after successive additions of small volumes of the concentrated H_2O_2 stock solution. From the obtained analytical curve (background-corrected cathodic current density *vs*. [H_2O_2]), the analytical parameters for H_2O_2 determination were recorded (linear concentration range, sensitivity and detection limit, LOD). The LOD was estimated from the equation $(3\ \sigma) / m$ (σ is the standard deviation obtained for the background current signal measured successively 10 times and m is the sensitivity (slope of the analytical curve)). The selectivity of the proposed NP-Pt(Au) sensor was evaluated from measurements carried out in the absence and presence of possible interfering biologically active redox species such as glucose, uric acid, ascorbic acid, and lactic acid at physiological concentration levels. Moreover, to evaluate the biofouling resilient features of the NP-Pt(Au) sensor, cyclic voltammetry and chronoamperometric measurements were taken in supporting electrolyte solution enriched by BSA (1.0 mg mL^{-1}). Analytical curves were constructed in the presence of BSA to effectively explore the anti-biofouling characteristics of the NP-Pt(Au) sensor in terms of analytical sensitivity.

3. Results and Discussion

3.1. Material characterization

The NP-Pt(Au) electrodes were prepared via the electrodeposition from a Pt and Ag salt solution onto a planar gold surface, as previously reported.[30] During the annealing step, the gold atoms from the underlying substrate diffuse into the electrodeposited thin film and mix with the Ag and Pt atoms to form a ternary metallic alloy film. The Ag is removed by dealloying in nitric acid and the Au/Pt is restructured during the dealloying process yielding a high surface area nanoporous Pt(Au) electrode.[30] Representative SEM images of the microscopic surface of the Pt(Au) electrode are shown in **Figure 1**. The surface of the nanoporous Pt(Au) electrode is rough and consists of islands/clusters at the film interface. Aggregates of nanorods with a sea-star-like structure were observed on the surface of the nanoporous electrode as depicted in **Figure 1A**. Under high SEM magnification (**Figure 1B**), small nanosized pores dispersed on the surface can be noted. Careful examination of these nanopores indicated the formation of hierarchical porous structure in which each mesopore is surrounded by a network of micropores. The morphology of the NP Pt(Au) materials is stable; we did not observe any change in morphology via AFM when these sensors are stored in air for 2-3 months.

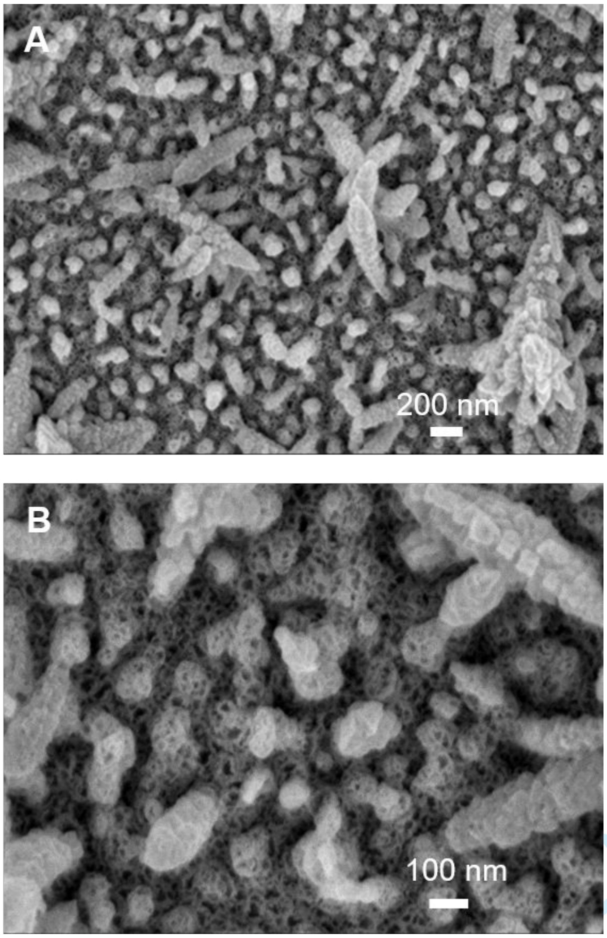

Figure 1. SEM images of NP-Pt (Au) at (A) low and (B) high magnification.

The electrodes were electrochemically characterized in terms of surface area from the evaluation of CVs acquired in sulfuric acid solution, 0.5 M H_2SO_4. **Figure 2** shows the CVs acquired at NP-Pt(Au) and planar Pt electrodes. The characteristic peaks for both platinum and gold can be noted for the NP-Pt(Au) electrode, indicating the presence of both metals in the porous film. The gold and platinum oxide peaks appear near +0.9 V and +0.4 V, respectively, and the platinum hydrogen adsorption/desorption peaks are near −0.15 V. Using the total charge associated with the hydrogen adsorption peaks near −0.15 V and the conversion factor 210 μC cm^{-2} [31-32] the electrochemically active surface area (ECSA) for NP-Pt(Au) was estimated to be 1.3 cm^2. From the obtained ECSA, the roughness factors (R_f

= ECSA/geometric area) of ~16 were determined for NP-Pt(Au). Similarly, the ECSA of NP-Pt(Au) with respect to the gold alloying metal was calculated. Thus, considering the total charge associated with the gold oxide reduction peak near +0.9 V and the conversion factor of 386 μC cm^{-2},[27, 32-33] respectively, the ECSA, in this case, was found to be 1.5 cm^{2}. This value is ~20 times higher than the electrode geometric area. The significant enhancement of surface area achieved for NP-Pt(Au) electrodes can be directly related to the large population of nanopores in the 3D bicontinuous framework.

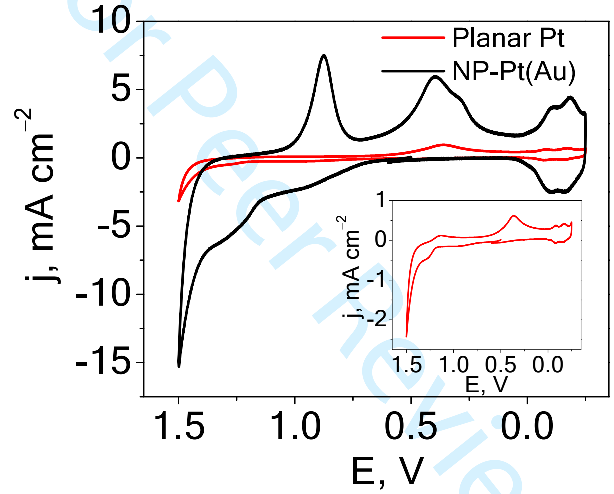

Figure 2. CVs in 0.5 M H_2SO_4 using planar Pt and NP-Pt(Au) electrodes. Scan rate = 50 mV/s. Inset: Amplification of CV acquired for a planar Pt electrode.

3.2. Hydrogen peroxide responsivity

The high surface area of bimetallic Pt(Au) alloy, together with its unique nanoporous structure and the presence of platinum should lend itself worthy to the electrochemical sensing of hydrogen peroxide, particularly in biofouling solutions. **Figures 3a,b** show CVs acquired at NP Pt(Au) and planar Pt electrodes in the presence and absence of hydrogen peroxide. It can be noted that the current density in buffer and buffer plus H_2O_2 is much larger at NP Pt(Au) relative to planar Pt. The high surface area increases both the capacitive and faradaic current resulting from the reduction of H_2O_2. It can also be noticed that the reduction of H_2O_2 at NP-Pt(Au) commences a few hundred millivolts (e.g., 263 mV) more positive than its reduction at a planar Pt electrode, **Figure 3c**. The presence of the small pores and/or step edges on the NP-Pt(Au) electrode's surface facilitates the electron transfer kinetics. A comparison to the results observed at nanoporous gold (NPG) prepared by chemical dealloying 12K gold leaf[34] is also shown in **Figure 3c.** As can be seen, a large overpotential is needed for the reduction of H_2O_2 at gold due to the slower electron transfer kinetics.

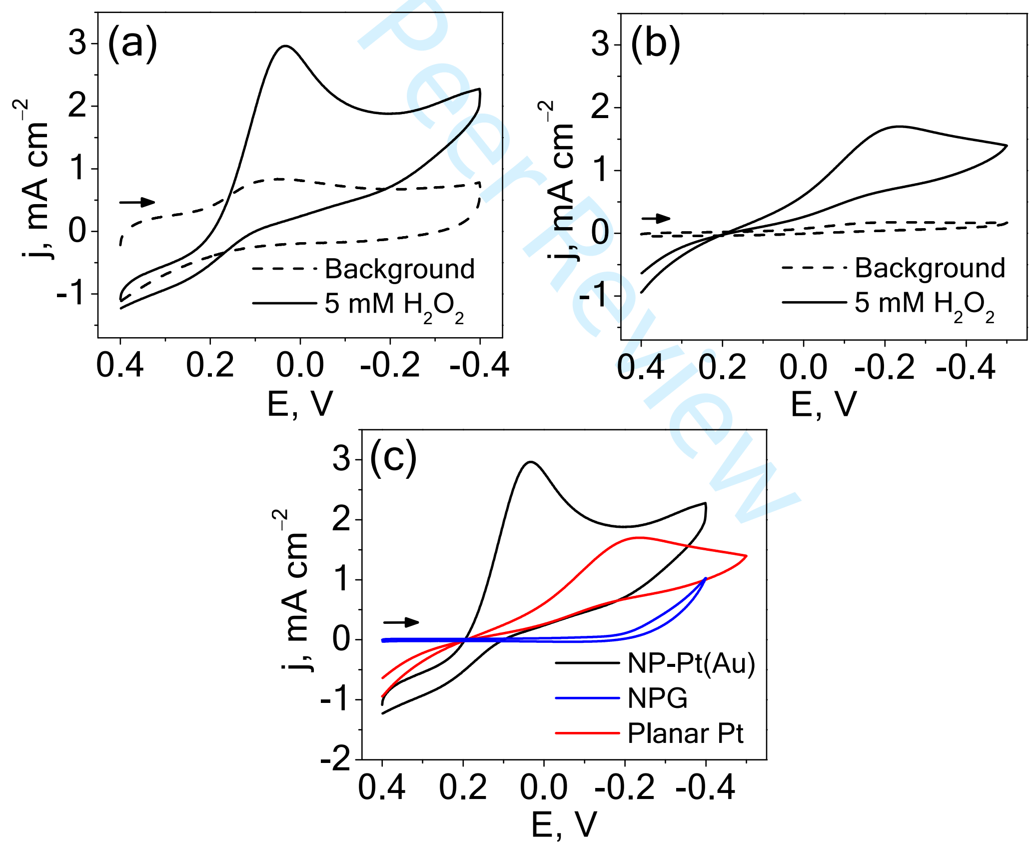

Figure 3. CVs obtained in 0.1 M phosphate buffer solution (pH 7.4) in the absence (background) and presence of 5.0 mM H_2O_2 using **(a)** NP-Pt(Au) and **(b)** planar Pt electrode. Scan rate = 50 mV/s. **(c)** Comparison of cyclic voltammograms obtained for 5.0 mM H_2O_2 using NP-Pt(Au), NPG, and planar Pt electrodes. Scan rate = 50 mV/s.

The dependence of the faradaic current on scan rate and concentration was also investigated. **Figure 4a** shows CVs recorded from 10 to 50 mV s^{-1}. The cathodic peak current density (Δj_p) increases linearly with scan rate ($v^{1/2}$) (**Figure 4a inset**), indicating the diffusion-controlled reduction of H_2O_2 at the NP-Pt(Au). In **Figure 4b**, CVs acquired at different concentrations are shown over the range of ~0.4 to 3.0 mM. The Faradaic current also varies linearly with the H_2O_2 concentration as noted in **Figure 4b inset**, suggesting that NP-Pt(Au) could be employed to carry out the direct non-enzymatic H_2O_2 electrochemical sensing.

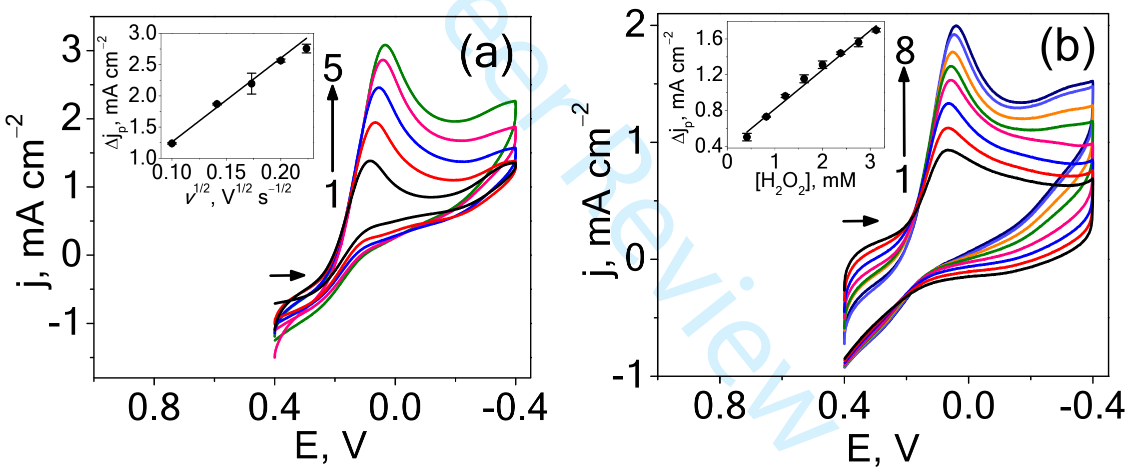

Figure 4. (a) CVs obtained at different scan rates (1: 10, 2: 20, 3: 30, 4: 40 and 5: 50 mV/s) in 0.1 M phosphate buffer (pH 7.4) containing 5.0 mM H_2O_2 at NP-Pt(Au). Inset: Plot of Δj_p *vs*. $v^{1/2}$. **(b)** CVs obtained in 0.1 M phosphate buffer solution (pH 7.4) containing different H_2O_2 concentrations (curve 1: 0.41 mM to curve 8: 3.1 mM) at NP-Pt(Au). Scan rate = 50 mV/s. Inset: Analytical curve for H_2O_2 (Δj_p *vs*. [H_2O_2]).

3.3. Biofouling studies

For electrochemical assays in complex solutions, biofouling of electrode surfaces can be problematic as it reduces the sensitivity of the electrode and increases detection limits. One unique feature of the NP-Pt(Au) electrodes described herein is the presence of small nanosized pores that are arranged in such a fashion that biosieving can take place. We and others have previously demonstrated that such electrodes (e.g., nanoporous gold[35]) are not as easily bio-fouled because large proteins cannot reach the inner electrode's surfaces while small redox molecules can.[27-29] **Figure 5** shows the CVs for the reduction of H_2O_2 at a planar Pt and NP-Pt(Au) electrodes before and after exposure to bovine serum albumin (BSA), which is known to passivate metal electrode surfaces.[25-26] At the planar Pt electrode, the peak for the reduction of H_2O_2 is immediately and significantly diminished and shifted to more negative potentials after exposure to albumin. This diminished response is indicative of the surface being fouled or passivated by the large protein molecules.[25-26] On NP-Pt(Au) electrode, however, negligible biofouling is observed. The faradaic peak for the reduction of H_2O_2 is nearly identical even after the electrode is exposed to albumin for 24 hours, demonstrating the excellent anti-biofouling features of these NP-Pt(Au) electrodes and again indicating the morphology of the electrode is stable when immersed in a solution. While we haven't determined the number of successive measurements that can be performed with the same Np-Pt(Au) using hydrogen peroxide as the analyte, our results obtained with potassium ferricyanide as the redox probe indicate at least 10 without the need to apply pretreatment/cleaning to the electrode between them.

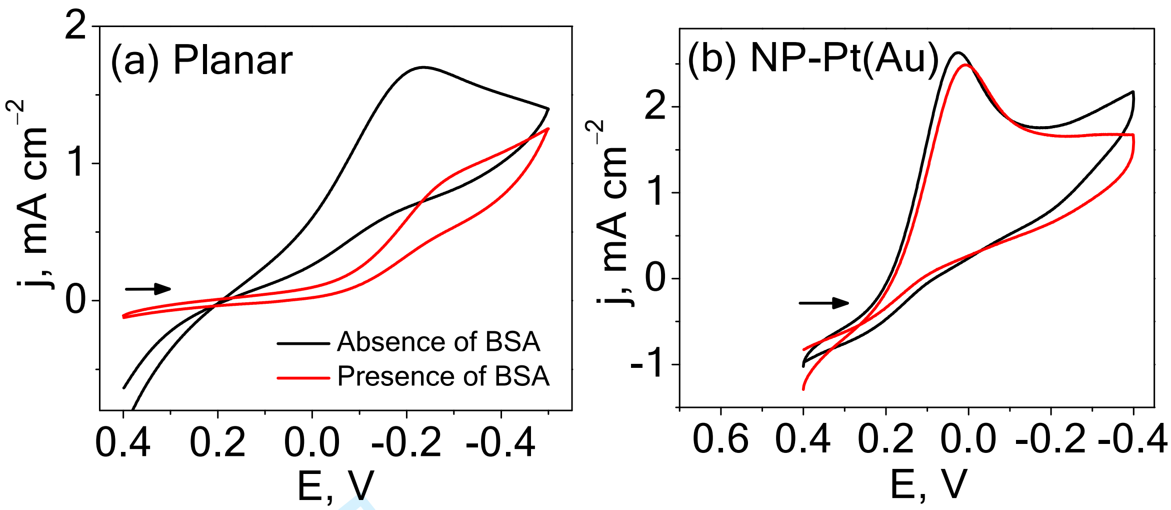

Figure 5. CVs obtained for 5.0 mM H_2O_2 in 0.1 M phosphate buffer solution (pH 7.4) in the absence and presence of 1.0 mg/mL BSA using **(a)** planar Pt and **(b)** NP-Pt(Au) electrodes. Scan rate = 50 mV/s.

The reproducibility in the electrochemical response of H_2O_2 acquired at five different electrodes is shown in **Figure 6**. Comparing the peak current densities, an RSD of 9.13% was obtained, indicating a good reproducibility between the electrochemical responses provided by different NP-Pt(Au) sensors.

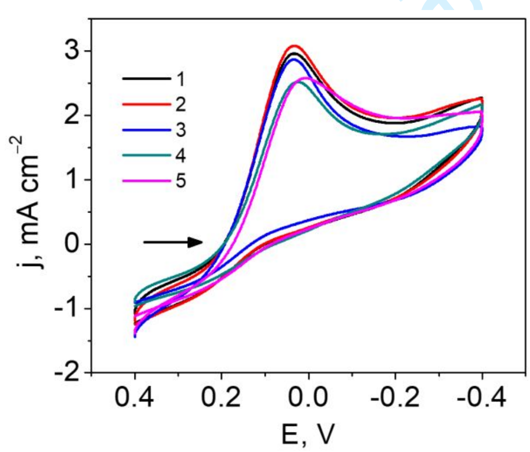

Figure 6. CVs obtained for 5.0 mM H_2O_2 in 0.1 M phosphate buffer solution (pH 7.4) using five different NP-Pt(Au) sensors. Scan rate = 50 mV/s.

3.4. Chronoamperometric determination of H_2O_2

Given the promising electrochemical and anti-biofouling properties of NP-Pt(Au) electrode towards the H_2O_2 reduction, its quantitative performance as an H_2O_2 electrochemical sensor was explored using chronoamperometry. For this, the applied potential for the determination of the target analyte H_2O_2 was −0.1 V *vs*. Ag/AgCl (0.1 M KCl). This potential was selected due to the desire to have the highly sensitive determination of H_2O_2 at the least negative potential possible. Once the applied potential has been selected, the chronoamperometric determination of H_2O_2 was carried out from successive injections of an H_2O_2 stock solution into the electrochemical cell to have different concentrations of the analyte. The chronoamperograms obtained in the H_2O_2 concentration range of 0.0709 to 1.25 mM are provided in **Figure 7a**. From the steady-current obtained through different concentrations of H_2O_2, the analytical curve for H_2O_2 (Δj *vs*. [H_2O_2]) was constructed (**Figure 7 b**). The analytical curve was linear according to the following linear regression equation, Eq. 1:

$$\Delta j\ (\mu A\ cm^{-2}) = -0.820\ \mu A\ cm^{-2} + 148\ \mu A\ cm^{-2}\ mM^{-1}\ [H_2O_2]\ (mM),\ r = 0.997 \qquad \text{Eq. 1}$$

From the obtained analytical sensitivity (148 $\mu A\ cm^{-2}\ mM^{-1}$), the LOD towards H_2O_2 was calculated to be 39.3 μM. The H_2O_2 chronoamperometric determination was also performed in the presence of BSA as a biofouling agent. The analytical curve obtained in the presence of 1 mg/mL BSA was constructed and the results are shown in **Figure 7b.** As can be seen, the analytical curve in the presence of BSA was linear over the same concentration range and presented a very similar slope to the one obtained without BSA (**Figure 7b inset**), suggesting the absence of any significant biofouling effect. This result is very promising, confirming the viability of these nanoporous electrodes for the electrochemical sensing of small molecules in complex matrice samples.

Table 1 displays a comparison of analytical parameters from different non-enzymatic electrochemical sensors for hydrogen peroxide reported in the current year. Non-enzymatic hydrogen peroxide detection has been achieved at different concentration levels, and the proposed sensor has competitive analytical performance relative to some recently designed modified electrodes. However, the highlight of our sensor platform is its anti-biofouling capacity, rarely systematically evaluated in other electrochemical devices. This is a very relevant aspect for practical applications in biological fluids, representing the most important novelty of our work in the field of bioanalysis.

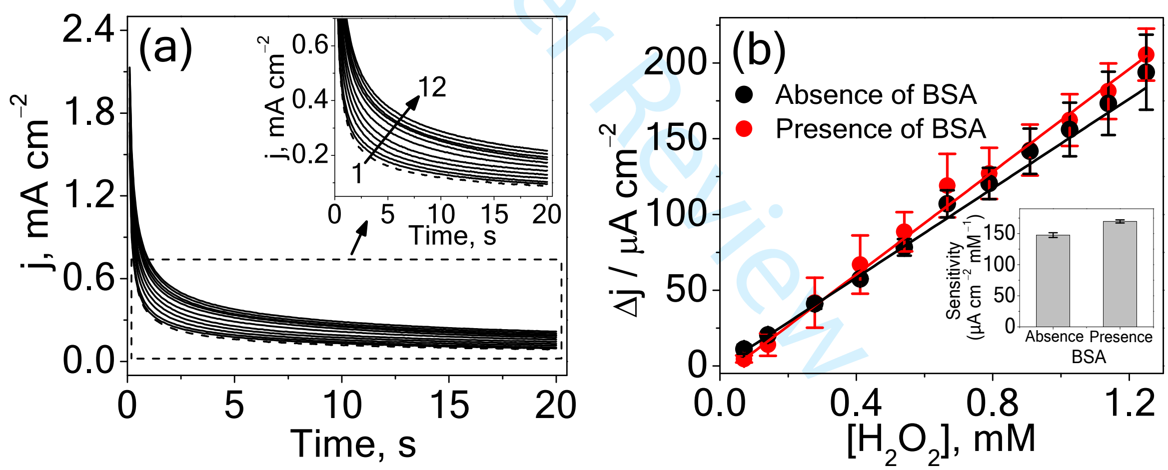

Figure 7. (a) Chronoamperometric curves obtained in 0.1 M phosphate buffer solution (pH 7.4) containing different H_2O_2 concentrations: curve 1: 0.0 (background), 2: 0.0709, 3: 0.141, 4: 0.278, 5: 0.411, 6: 0.540, 7: 0.667, 8: 0.789, 9: 0.909, 10: 1.02, 11: 1.14 and curve 12: 1.25 mM) using NP-Pt(Au) electrode. Applied potential: −0.1 V *vs*. Ag/AgCl (0.1 M KCl). **(b)** Analytical curve obtained for H_2O_2 in the presence (black line) and absence (red line) of BSA (1 mg/mL) at NP-Pt(Au) electrode. The current was background-corrected and obtained at

−0.1 V at 20 seconds after the potential step. Inset: Comparison of analytical sensitivities towards H_2O_2 obtained in the absence and presence of BSA.

Table 1. Comparison of analytical parameters recorded by non-enzymatic electrochemical sensors towards H_2O_2 determination during the past year

Electrode	Linear range (mM)	LOD (μM)	Biofouling tests	Reference
Zn_2GeO_4 rods	0.001 to 4.0	0.1	No	[36]
$CuBi_2O_4$/FTO	0.2 to 2.6	380	No	[37]
dBPN	0.005 to 6.955 and 6.955 to 24.955	4.11	No	[38]
rGO	0.215 to 24.955	202.45	No	[38]
NiCo LDH/GCE	2.0×10^{-5} to 11.5	0.0044	No	[39]
CuO/g-C_3N_4/GCE	5.0×10^{-4} to 0.05	0.31	No	[40]
AuNPs-PB-GO/GCE	0.0038 to 5.4	1.3	No	[41]
PBNPs@AuNWs	5.0×10^{-5} to 0.1623	0.0053	No	[42]
$CuGa_2O_4$/GCE	0.05 to 2.0	25	No	[43]
MoO_3–MoS_2/PPy	3.0×10^{-4} to 0.15	0.18	No	[44]
Cu–MoO_2/C/GCE	2.4×10^{-4} to 4.27	0.085	No	[45]
Fe_3O_4@PDA-Ag	0.1 to 17	1.6	No	[46]
NP-Pt(Au)	0.0709 to 1.25	39.3	Yes	This work

dBPN: defective black phosphorus nanosheets, rGO: reduced graphene oxide, FTO: fluorine-doped tin oxide, NiCo LDH: flower-like NiCo layered double hydroxides, GCE: glassy carbon electrode, AuNPs: gold nanoparticles, PB: Prussian blue, GO: graphene oxide, MoO_3–MoS_2/PPy: molybdenum oxide-molybdenum disulfide-containing polypyrrole self-supporting hollow flexible electrode, and PDA: Polydopamine.

3.5. Selectivity tests and sample analysis

The sensor selectivity in the presence of some of the chemical substances typically found in biological fluids was investigated. The chronoamperometric response of NP-Pt(Au) electrode towards H_2O_2 was interrogated in supporting electrolyte containing glucose, uric acid, ascorbic acid, or lactic acid at physiological concentration levels. In **Figures 8a-d,** the chronoamperograms recorded in the presence of each of these substances are shown. As can be seen, the registered Faradaic cathodic currents were nearly constant after the addition of the possible interfering substances. The relative standard deviations (RSDs) showed in **Table 2** were obtained from the comparison of H_2O_2 cathodic current obtained in the absence and presence of the interfering species. The low values of RSDs ranging from −6.5 to +5.0% were indicative of NP-Pt(Au) selective performance relative to the four species evaluated.

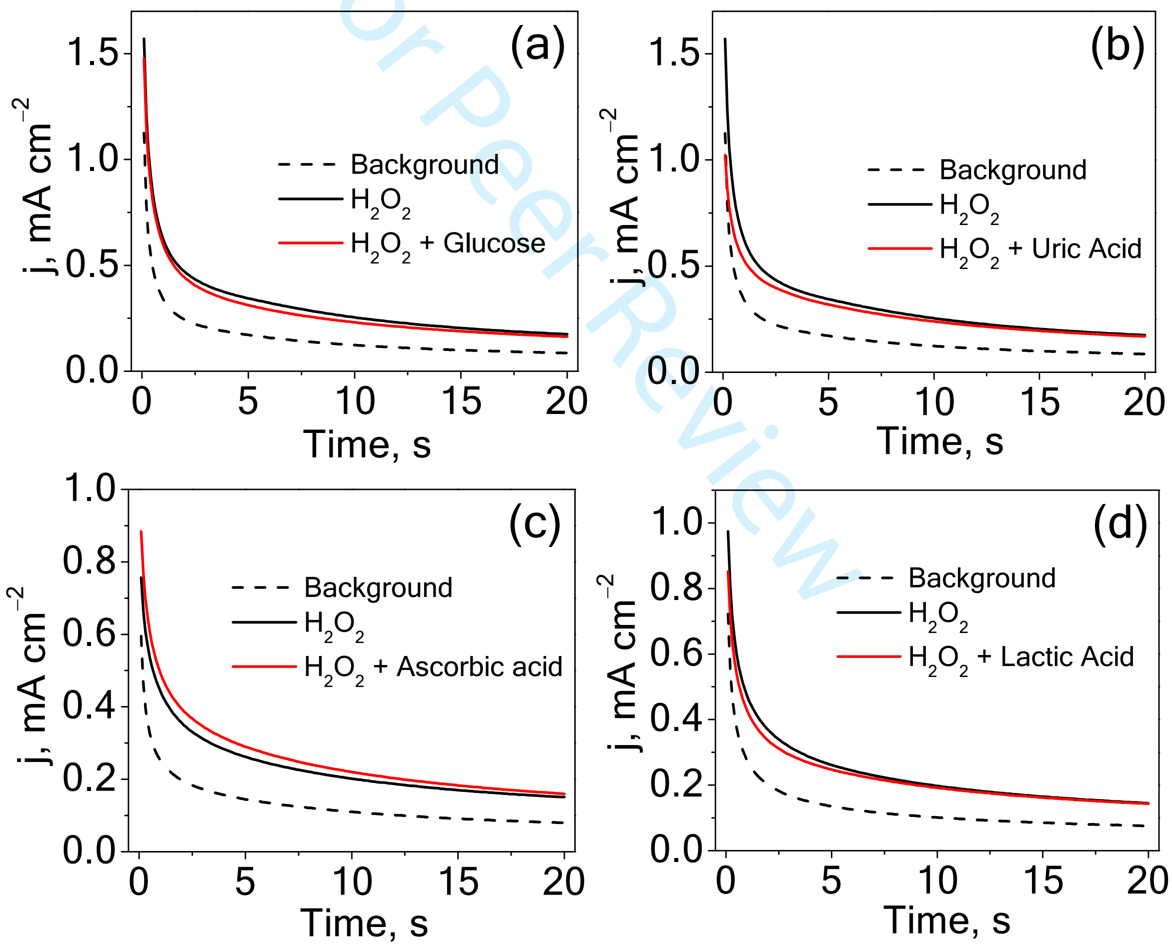

Figure 8. Chronoamperometric curves obtained for 0.67 mM H_2O_2 in 0.1 M phosphate buffer solution (pH 7.4) in the absence and presence of **(a)** 5.0 mM glucose, **(b)** 0.1 mM uric acid, **(c)** 0.05 mM ascorbic acid and **(d)** 1.5 mM lactic acid using NP-Pt(Au) electrode. Applied potential: −0.1 V vs. Ag/AgCl (0.1 M KCl).

Table 2. RSD values obtained in the study of interferents.

Interfering specie	RSD (%)
Glucose	−1.4
Uric acid	−6.5
Ascorbic acid	+5.0
Lactic acid	−3.8

The proposed NP-Pt(Au) sensor was then applied for the H_2O_2 determination in a complex biological matrix, namely fetal bovine serum (FBS) sample. Following the methodology of Seker and collaborators,[29, 47-48] a 10% (v/v) FBS sample was prepared in 0.1 M phosphate buffer solution (pH 7.4) and spiked with a known concentration of H_2O_2 (0.14 mM). The chronoamperograms were recorded for the unspiked (background recording) and spiked samples. By interpolation of the background-corrected cathodic currents in the respective analytical curve, the added H_2O_2 concentration was recovered: 0.148 ± 0.003 mM, $n = 3$; which gives an excellent recovery percentage of 105.7%. This result demonstrated the applicability and importance of the NP-Pt(Au) nanoporous morphology in ensuring the successful determination of hydrogen peroxide at biological matrices rich in fouling agents.

4. Conclusions

Nanoporous Pt(Au) electrodes were fabricated, characterized, and successfully utilized in the determination of hydrogen peroxide in simple buffer solutions, in buffered solutions containing the known biofouling agent, BSA, and in a complex solution, FBS. Compared to nanoporous gold electrodes, H_2O_2 can more easily be reduced at NP Pt(Au) while maintaining the same biosieving capabilities in the presence of albumin due to its unique 3D nanoporous framework. Using chronoamperometry, a limit of detection of 39 μM was obtained. Although the detection limits are not quite as small as some recently published work using 'designer' electrodes, the electrodes fabricated herein are relatively simple and can make such measurements in complex biological solutions with little to no loss in their sensitivity. Further improvements in the detection limits by using either square wave or differential pulse voltammetry are recommended to better discriminate against the non-Faradaic current. Such improvements in detection limit will be necessary for such electrodes to be used to detect the low to sub-micromolar concentrations of hydrogen peroxide in biological samples.[49] Future directions will proceed in this avenue.

5. Acknowledgements

This study was financed in part by the Coordenação de Aperfeiçoamento de Pessoal de Nível Superior - Brasil (CAPES) - Finance Code 001.

6. Conflict of interest statement

MMC has an invention disclosure submitted to VCU on the platinum-gold bimetallic alloys used in this work.

7. Data Availability Statement

The data that support the findings of this study are available from the corresponding author upon reasonable request.

List of Tables and Figures legend:

Table 1. Comparison of analytical parameters recorded by non-enzymatic electrochemical sensors towards H_2O_2 determination during the past year

Table 2. RSD values obtained in the study of interferents.

Figure 1. SEM images of NP-Pt (Au) at (A) low and (B) high magnification.

Figure 2. CVs in 0.5 M H_2SO_4 using planar Pt and NP-Pt(Au) electrodes. Scan rate = 50 mV/s. Inset: Amplification of CV acquired for a planar Pt electrode.

Figure 3. CVs obtained in 0.1 M phosphate buffer solution (pH 7.4) in the absence (background) and presence of 5.0 mM H_2O_2 using **(a)** NP-Pt(Au) and **(b)** planar Pt electrode. Scan rate = 50 mV/s. **(c)** Comparison of cyclic voltammograms obtained for 5.0 mM H_2O_2 using NP-Pt(Au), NPG, and planar Pt electrodes. Scan rate = 50 mV/s.

Figure 4. (a) CVs obtained at different scan rates (1: 10, 2: 20, 3: 30, 4: 40 and 5: 50 mV/s) in 0.1 M phosphate buffer (pH 7.4) containing 5.0 mM H_2O_2 at NP-Pt(Au). Inset: Plot of Δj_p *vs*. $v^{1/2}$. **(b)** CVs obtained in 0.1 M phosphate buffer solution (pH 7.4) containing different H_2O_2 concentrations (curve 1: 0.41 mM to curve 8: 3.1 mM) at NP-Pt(Au). Scan rate = 50 mV/s. Inset: Analytical curve for H_2O_2 (Δj_p *vs*. [H_2O_2]).

Figure 5. CVs obtained for 5.0 mM H_2O_2 in 0.1 M phosphate buffer solution (pH 7.4) in the absence and presence of 1.0 mg/mL BSA using **(a)** planar Pt and **(b)** NP-Pt(Au) electrodes. Scan rate = 50 mV/s.

Figure 6. CVs obtained for 5.0 mM H_2O_2 in 0.1 M phosphate buffer solution (pH 7.4) using five different NP-Pt(Au) sensors. Scan rate = 50 mV/s.

Figure 7. (a) Chronoamperometric curves obtained in 0.1 M phosphate buffer solution (pH 7.4) containing different H_2O_2 concentrations: curve 1: 0.0 (background), 2: 0.0709, 3: 0.141, 4: 0.278, 5: 0.411, 6: 0.540, 7: 0.667, 8: 0.789, 9: 0.909, 10: 1.02, 11: 1.14 and curve 12: 1.25 mM) using NP-Pt(Au) electrode. Applied potential: −0.1 V *vs*. Ag/AgCl (0.1 M KCl). **(b)** Analytical curve obtained for H_2O_2 in the presence (black line) and absence (red line) of BSA (1 mg/mL) at NP-Pt(Au) electrode. The current was background-corrected and obtained at −0.1 V at 20 seconds after the potential step. Inset: Comparison of analytical sensitivities towards H_2O_2 obtained in the absence and presence of BSA.

Figure 8. Chronoamperometric curves obtained for 0.67 mM H_2O_2 in 0.1 M phosphate buffer solution (pH 7.4) in the absence and presence of **(a)** 5.0 mM glucose, **(b)** 0.1 mM uric acid,

(c) 0.05 mM ascorbic acid and **(d)** 1.5 mM lactic acid using NP-Pt(Au) electrode. Applied potential: −0.1 V vs. Ag/AgCl (0.1 M KCl).

7. References

[1] K. Dhara, D. R. Mahapatra, *Journal of Materials Science* **2019**, *54*, 12319-12357.
[2] W. Chen, S. Cai, Q.-Q. Ren, W. Wen, Y.-D. Zhao, *Analyst* **2012**, *137*, 49-58.
[3] H. Sies, *Journal of Biological Chemistry* **2014**, *289*, 8735-8741.
[4] H. Liu, L. Weng, C. Yang, *Microchimica Acta* **2017**, *184*, 1267-1283.
[5] C. J. McDonnell-Worth, D. R. MacFarlane, *Australian Journal of Chemistry* **2018**, *71*, 781-788.
[6] J. Meier, E. M Hofferber, J. A Stapleton, N. M Iverson, *Chemosensors* **2019**, *7*, 64.
[7] V. Patel, P. Kruse, P. R. Selvaganapathy, *Biosensors* **2021**, *11*, 9.
[8] X. Chen, G. Wu, Z. Cai, M. Oyama, X. Chen, *Microchimica Acta* **2014**, *181*, 689-705.
[9] S. Park, H. Boo, T. D. Chung, *Analytica chimica acta* **2006**, *556*, 46-57.
[10] H. Shamkhalichenar, J.-W. Choi, *Journal of the Electrochemical Society* **2020**, *167*, 037531.
[11] K. E. Toghill, R. G. Compton, *Int. J. Electrochem. Sci* **2010**, *5*, 1246-1301.
[12] F. Meng, X. Yan, J. Liu, J. Gu, Z. Zou, *Electrochimica Acta* **2011**, *56*, 4657-4662.
[13] Y. J. Lee, J. Y. Park, Y. Kim, J. W. Ko, *Current Applied Physics* **2011**, *11*, 211-216.
[14] R. Zeis, T. Lei, K. Sieradzki, J. Snyder, J. Erlebacher, *Journal of Catalysis* **2008**, *253*, 132-138.
[15] S. A. Evans, J. M. Elliott, L. M. Andrews, P. N. Bartlett, P. J. Doyle, G. Denuault, *Analytical Chemistry* **2002**, *74*, 1322-1326.
[16] J. Wang, H. Gao, F. Sun, C. Xu, *Sensors and Actuators B: Chemical* **2014**, *191*, 612-618.
[17] D. Thatikayala, D. Ponnamma, K. K. Sadasivuni, J.-J. Cabibihan, A. K. Al-Ali, R. A. Malik, B. Min, *Biosensors* **2020**, *10*, 151.
[18] S. Chen, R. Yuan, Y. Chai, F. Hu, *Microchimica Acta* **2013**, *180*, 15-32.
[19] R. Zhang, W. Chen, *Biosensors and Bioelectronics* **2017**, *89*, 249-268.
[20] S. B. Hall, E. A. Khudaish, A. L. Hart, *Electrochimica Acta* **1998**, *43*, 579-588.
[21] S. B. Hall, E. A. Khudaish, A. L. Hart, *Electrochimica Acta* **1998**, *43*, 2015-2024.
[22] A. Barfidokht, J. J. Gooding, *Electroanalysis* **2014**, *26*, 1182-1196.
[23] S. G. Roscoe, K. L. Fuller, *Journal of Colloid and Interface Science* **1992**, *152*, 429-441.
[24] N. Wisniewski, F. Moussy, W. M. Reichert, *Fresenius Journal of Analytical Chemistry* **2000**, *366*, 611-621.
[25] P. Ying, A. S. Viana, L. M. Abrantes, G. Jin, *Journal of colloid and interface science* **2004**, *279*, 95-99.
[26] S. E. Moulton, J. N. Barisci, A. Bath, R. Stella, G. G. Wallace, *Journal of Colloid and Interface Science* **2003**, *261*, 312-319.
[27] A. A. Farghaly, M. Lam, C. J. Freeman, B. Uppalapati, M. M. Collinson, *Journal of The Electrochemical Society* **2016**, *163*, H3083-H3087.
[28] J. Patel, L. Radhakrishnan, B. Zhao, B. Uppalapati, R. C. Daniels, K. R. Ward, M. M. Collinson, *Analytical chemistry* **2013**, *85*, 11610-11618.

[29] P. Daggumati, Z. Matharu, L. Wang, E. Seker, *Analytical Chemistry* **2015**, *87*, 8618-8622.
[30] A. A. Farghaly, R. K. Khan, M. M. Collinson, *ACS applied materials & interfaces* **2018**, *10*, 21103-21112.
[31] S. Trasatti, O. Petrii, *Pure and applied chemistry* **1991**, *63*, 711-734.
[32] M. Łukaszewski, M. Soszko, A. Czerwiński, *Int. J. Electrochem. Sci* **2016**, *11*, 4442-4469.
[33] A. A. Farghaly, M. M. Collinson, *Langmuir* **2014**, *30*, 5276-5286.
[34] T. A. Silva, M. R. K. Khan, O. Fatibello-Filho, M. M. Collinson, *Journal of Electroanalytical Chemistry* **2019**, *846*, 113160.
[35] E. Seker, M. L. Reed, M. R. Begley, *Materials* **2009**, *2*, 2188-2215.
[36] N. Fan, Q. Kong, R. Lang, H. Guan, G. Chen, C. Dong, *Surfaces and Interfaces* **2021**, *25*, 101295.
[37] G. N. Sinha, P. Subramanyam, V. Sivaramakrishna, C. Subrahmanyam, *Inorganic Chemistry Communications* **2021**, *129*, 108627.
[38] T.-P. Wang, C.-L. Lee, C.-H. Kuo, W.-C. Kuo, *Applied Surface Science* **2021**, *542*, 148588.
[39] M. Annalakshmi, S. Kumaravel, T.-W. Chen, S.-M. Chen, B.-S. Lou, *ACS Applied Bio Materials* **2021**, *4*, 3203-3213.
[40] K. Atacan, M. Özacar, *Materials Chemistry and Physics* **2021**, *266*, 124527.
[41] X. Liu, X. Zhang, J. Zheng, *Microchemical Journal* **2021**, *160*, 105595.
[42] K. Zhang, Z. Zhang, X. Zhou, N. Zhang, *Electroanalysis* **2021**, *33*, 1167-1174.
[43] H. Yin, Y. Shi, Y. Dong, X. Chu, *Journal of Electroanalytical Chemistry* **2021**, *885*, 115100.
[44] P. Cao, N. Wang, H. Dai, H. Ma, M. Lin, *Analytica Chimica Acta* **2021**, *1151*, 338251.
[45] B. Li, L.-H. Liu, X.-F. Zhang, Y. Gao, Z.-P. Deng, L.-H. Huo, S. Gao, *Analytica Chimica Acta* **2021**, *1143*, 73-83.
[46] M. Luo, Y. Zhang, S. Zhao, *Journal of The Electrochemical Society* **2021**.
[47] P. Daggumati, S. Appelt, Z. Matharu, M. L. Marco, E. Seker, *Journal of the American chemical society* **2016**, *138*, 7711-7717.
[48] Z. Matharu, P. Daggumati, L. Wang, T. S. Dorofeeva, Z. Li, E. Seker, *ACS applied materials & interfaces* **2017**, *9*, 12959-12966.
[49] H. J. Forman, A. Bernardo, K. J. Davies, *Archives of Biochemistry and Biophysics* **2016**, *603*, 48-53.